

Mineralogy of Pb-P grains in the roots of *Agrostis capillaris* L. by ATEM and EXAFS*

J. D. COTTER-HOWELLS^{1,2,†}, P. E. CHAMPNESS¹ AND J. M. CHARNOCK^{1,3}

¹ Department of Earth Sciences, The University of Manchester, Manchester M13 9PL, UK

² School of Biological Sciences, The University of Manchester, Manchester M13 9PL, UK

³ CLRC Daresbury Laboratory, Warrington WA4 4AD, UK

ABSTRACT

Analytical transmission electron microscopy (ATEM) and X-ray absorption spectroscopy (XAS) have been used to determine the mineralogy of Pb-P deposits in the roots of the heavy metal tolerant grass cultivar *Agrostis capillaris* L. cv. Parys Mountain. The deposits have a pyromorphite ($\text{Pb}_5(\text{PO}_4)_3\text{Cl}$)-type structure and composition although some of the Cl may be substituted by OH. Energy-dispersive mapping under the scanning electron microscope demonstrated that the majority of these deposits are present in the outer cell wall of the epidermis (the outermost layer of root cells). The phosphate composition of these grains contrasts with the phytate ($\text{C}_6\text{H}_{18}\text{O}_{24}\text{P}_6^{12-}$) composition of Zn-P deposits observed in similar electron microscopy studies. The physiological role of heavy metal P deposits is unclear. Heavy metal P precipitates may form actively as a tolerance mechanism to heavy metals or passively, sequestering P in a metabolically inactive form.

KEYWORDS: lead, lead phosphate, pyromorphite, lead hydroxyapatite, electron microscopy, electron diffraction, heavy metal tolerance, *Agrostis capillaris*.

Introduction

Metal phosphates are generally sparingly soluble and stable over a wide range of geochemical conditions. Calcium, Al and Fe phosphates commonly occur as trace minerals in soils and sediments, both as primary precipitates and inherited minerals (Nriagu and Moore, 1984). In addition, Pb and Zn phosphates are known to form in heavy metal contaminated soils (Davis *et al.*, 1993; Ruby *et al.*, 1994; Cotter-Howells *et al.*, 1994; Cotter-Howells, 1996; Cotter-Howells and Caporn, 1996). The extremely poor solubilities of

these minerals (e.g. $K_{sp} = 10^{-84.4}$ for pyromorphite, $\text{Pb}_5(\text{PO}_4)_3\text{Cl}$ and $K_{sp} = 10^{-35.3}$ for hopeite, $\text{Zn}_3(\text{PO}_4)_2 \cdot 4\text{H}_2\text{O}$) are thought to be important in maintaining low aquatic concentrations of these two heavy metals in the surface environment (Nriagu, 1974; 1984). Several studies have now advocated the formation of pyromorphite and/or Pb-hydroxyapatite, its hydroxy analogue, as a technique for removing Pb from waste waters by precipitation from apatite, $\text{Ca}_5(\text{PO}_4)_3\text{OH}$ (Ma *et al.*, 1995) and as a soil remediation technology, rendering Pb in an insoluble form (Ruby *et al.*, 1994; Cotter-Howells and Caporn, 1996; Cotter-Howells, 1996).

Phosphorus is an essential plant macronutrient. It is a structural element in nucleic acids and phospholipids (which form biomembranes regulating solute uptake into cells). It is commonly stored within plant cells, seeds and grains as Ca polyphosphate (phosphate polymer) granules or as phytate salt deposits, typically K, Mg, Ca salts of phytic acid, myoinositol, 1,2,3,4,5,6-hexakisphosphate, $\text{H}_{12}\text{C}_6\text{H}_{18}\text{O}_{24}\text{P}_6$ (Marschner, 1995). This

* The first four papers in this issue were presented at the Mineralogical Society's Spring Meeting, held on 18th March 1997, entitled 'Phosphates: biogenic to exotic'

† Present address: Department of Plant and Soil Science, Cruickshank Building, Aberdeen University, Aberdeen AB24 3UU, UK.

stored P can be remobilized and transported in the plant sap. This remobilization, together with the initial uptake of P, leads to a considerable movement of P in the aqueous phase of plants. If aqueous heavy metals are also taken up into plants (e.g. when grown in heavy metal contaminated land), it is conceivable that interactions between heavy metals and P may occur in plants in a similar fashion to those known to occur in the soil.

Several studies have observed the occurrence of heavy metal P precipitates in the roots and leaves of plants that have been exposed to elevated concentrations of Zn, Cd or Pb. These studies have used scanning electron microscopy (SEM) combined with energy dispersive X-ray (EDX) analysis and/or analytical transmission electron microscopy (ATEM), i.e. TEM combined with EDX. Elemental ratios obtained by EDX analysis of Zn-rich P globules in the roots of Zn tolerant *Deschampsia cespitosa* (L.) P. Beauv. and *Lemna minor* L. led van Steveninck *et al.* (1987a; 1987b; 1990) to conclude that these precipitates were probably K or Mg phytate with up to 60% site occupancy by Zn. However, phytates are not generally crystalline (J. Cotter-Howells, unpubl. data) which makes definitive identification within plants difficult. Vázquez *et al.* (1994) concluded that Zn-P deposits found in the roots and leaves of the metal hyperaccumulator *Thlaspi caerulescens* J. & C. Presl. were crystalline and not Zn phytate. Turnau *et al.* (1993) found Cd associated with polyphosphate granules in the roots of bracken (*Pteridium aquilinum* L.) infected with a symbiotic fungus (mycorrhiza). An early study by Malone *et al.* (1974) reported crystalline Pb deposits on and within the roots of maize (*Zea mays* L.) but did not identify the crystals. A more recent study by Cotter-Howells and Caporn (1996) reported the presence of Pb-P deposits in soil removed by ultrasound from the outer surfaces of the roots (the rhizosphere) of a heavy metal tolerant grass, *Agrostis capillaris* L. cv. Parys Mountain that had been grown on soil contaminated by mine-waste. Qualitative EDX spectra obtained from Pb-P grains were consistent with pyromorphite ($\text{Pb}_5(\text{PO}_4)_3\text{Cl}$), but the small size of the grains (~1 µm diameter) precluded quantitative EDX analysis.

Although several of these heavy metal P deposits have been described as crystalline, the exact mineralogical identity of these precipitates remains unknown due to a lack of micro-

mineralogical studies. This prevents a full understanding of the physiological role of these deposits within plants. The present micro-mineralogical study describes further the Pb-P deposits, associated with the roots of *A. capillaris*, found by Cotter-Howells and Caporn (1996) and discusses their possible physiological significance.

Methodology

A bulk sample of soil contaminated by mine-waste from Van mine in mid-Wales and containing 10.9 g Pb kg⁻¹ was amended with peat to give 10% dry weight organic matter. Seeds of *A. capillaris* cv. Parys Mountain were sown directly onto the soil surface as described by Cotter-Howells and Caporn (1996) and the plants were harvested after three months. The spatial distribution of Pb-P deposits within roots was determined using SEM combined with EDX mapping. To determine the mineralogy of Pb-P grains, root samples were analysed by analytical transmission electron microscopy (ATEM) and X-ray absorption spectroscopy (XAS).

Sample preparation

Root samples were prepared in several different ways according to the requirements of each analytical technique used. For bulk chemical analysis, 0.1 g of root was washed thoroughly with de-ionized water (DIW), freeze-dried and then subjected to a nitric/perchloric (4:1) acid digestion.

Cubes of root and soil (~0.1 cm³ in size) were freeze-dried and impregnated with epoxy resin under vacuum so that the location of Pb-P deposits could be investigated. Sections were cut from the impregnated blocks and polished using diamond paste to give 30 µm thickness. Initial examination using SEM indicated that the Pb-P grains were associated with plant roots rather than the soil. Therefore, further SEM work was performed solely on the roots of *A. capillaris*. Roots were washed in DIW to remove soil particles. Individual roots were then isolated, cut into 5 mm lengths and chemically fixed in 2.5% glutaraldehyde in 0.1 M sodium cacodylate buffer (pH 7.2–7.4) overnight at 4°C. No post-fixation or staining agents were used as these might interfere with EDX mapping. Samples were impregnated with Spurr's resin after progressive replacement of water with ethanol. Transverse cross-sections (5 µm thick) were mounted on a

glass slide and coated with carbon in preparation for SEM analysis.

Ion-beam (Ar^+) thinned sections of roots were made from further 30 μm thick sections cut from the freeze-dried embedded block of soil and roots (see above). As ultra-microtoming could alter the morphology and possibly result in loss of precipitates, ion-thinned sections were used for initial ATEM investigations. Because of difficulties encountered in obtaining diffraction patterns suitable for mineral identification, roots were also ashed to liberate the Pb-P grains. Dried root (0.1 g) was ashed at 400°C for 8 h and the resulting ash dispersed in water onto a carbon-coated copper grid suitable for ATEM. To determine whether pyromorphite was stable at the ashing temperature, a sample of synthetic pyromorphite was subjected to X-ray powder diffraction (XRD) before and after heating at 400°C for 8 h. The XRD trace showed no change, demonstrating that pyromorphite is stable at the ashing temperature.

For XAS analysis, bulk samples of roots were washed gently with DIW, freeze-dried and ground to a powder.

Model compounds for XAS and ATEM consisted of samples of pyromorphite and Pb-hydroxyapatite synthesized as follows. For pyromorphite ($\text{Pb}_5(\text{PO}_4)_3\text{Cl}$), solutions containing 250 ml 0.5 M PbNO_3 and 250 ml of 0.3 HNa_2PO_4 and 0.1 M NaCl were heated to boiling, mixed, and stirred overnight whilst cooling. The mixture was then filtered and the precipitate washed several times in DIW and dried at 100°C. Similarly, Pb-hydroxyapatite ($\text{Pb}_5(\text{PO}_4)_3\text{OH}$) was synthesized using solutions containing 250 ml 0.5 M $(\text{CH}_3\text{COO})_2\text{Pb}$ and 250 ml of 0.3 HNa_2PO_4 . The structure and purity of the model compounds were verified by XRD.

Analysis

Bulk chemical analysis of roots

The acid-digested samples were analysed by atomic absorption spectrophotometry (AAS) for Pb and by spectrometry at 882.0 nm for P using the molybdenum blue method (Allen, 1989). Analytical quality controls (blanks, standards and duplicates) indicated the analytical error to be better than $\pm 15\%$ for both Pb and P.

EDX mapping

The EDX mapping was performed using a JEOL 6400 scanning electron microscope oper-

ating at 20 kV and 1.5 nA. Elemental windows for Pb and P of 100 eV width were predetermined using the synthetic pyromorphite standard. Chlorine was not mapped as it is a constituent of Spurr's resin. Back-scattered images (BSI) showing atomic number contrast were collected simultaneously.

ATEM

A Philips EM430 TEM operating at 300 kV was employed for the imaging and diffraction experiments. The energy-dispersive spectra were recorded in a Phillips CM200 TEM operating at 200 kV. The microscope is fitted with a Tracor-Northern thin window detector. An EDAX DX4 system with MDX software was used to obtain integrated peak intensities. The morphology of Pb-P grains was examined in ion-thinned samples and electron diffraction patterns were observed that indicated crystalline material with a pyromorphite-like structure. However, the high voltages necessary for electron diffraction induced beam damage in organic material making the sample unstable. In addition, it was difficult to find grains of suitable thickness for selected area electron diffraction (SAED) in these samples. Therefore, SAED and EDX analyses were performed on liberated Pb-bearing grains in ashed samples of roots. In addition EDX analyses were performed on grains of the synthetic pyromorphite standard dispersed onto a carbon-coated copper grid. The camera constant was determined using an evaporated-gold standard.

XAS

X-ray absorption spectra at the Pb L(III)-edge were collected at room temperature on Station 7.1 at the Daresbury Synchrotron Radiation Source (SRS) operating at 2 GeV with an average current of 150 mA, using a Si (111) double crystal monochromator, detuned to reject 50% of the beam in order to minimize harmonic contamination. Data for the freeze-dried plant roots were collected from ~ 0.1 g of material mounted on Sellotape in an Al sample holder, with the station operating in fluorescence mode using a solid state NaI scintillation detector. Nineteen scans were taken and averaged to improve the signal to noise ratio. Data for selected Pb model compounds were collected as single scans in transmission mode. Details of the background subtraction and fitting procedures can be found in Charnock (1995); a smoothly varying background was subtracted

from the raw adsorption spectrum and the amplitude of the EXAFS oscillations was normalized to the size of the edge step. The oscillations, denoted χ , are expressed as a function of the electron wave vector, k . A Fourier transform of the EXAFS spectrum provides an approximate radial distribution around the absorber atom (Pb), giving a peak for each shell of scatterers. A theoretical spectrum was then generated and fitted to the experimental spectrum in EXCURV92 (Binsted *et al.*, 1991) using *ab initio* calculated phaseshifts. The absorber-scatterer distances and Debye-Waller factors were refined to obtain the best fit, indicated by the lowest R-factor (Binsted *et al.*, 1992).

Results

Bulk chemical analysis of roots

The total concentrations of Pb and P in the bulk roots were 1.29 mg g⁻¹ and 1.44 mg g⁻¹, respectively, expressed on a dry weight basis.

EDX mapping

The BSI maps (Fig. 1*a,b*) indicate the presence of grains containing an element of high atomic number. Comparison of EDX maps with BSI maps clearly demonstrates that these grains contain both Pb and P. Whilst all Pb-bearing grains contain P, there are some grains that contain P but for which Pb is absent. These grains must be a different P-containing compound, possibly an Fe or Al phosphate, but are too small for individual analysis. The Pb-P grains occur mostly on the surface of the root or in the outer wall of the epidermis (the outermost layer of root cells), whilst relatively few grains are present in the root cortex (inner root cells). Those that are present in the cortex tend to be extra-cellular, i.e. in the cell walls rather than within the cell.

ATEM

The Pb-P grains were located by qualitative EDX analysis in ion-thinned sections and often contained minor amounts of Fe and Zn. The morphology of grains is the same in both ion-thinned and ashed samples, confirming that these deposits are stable at the ashing temperature. However, the spatial relationship of the Pb-P grains to the structure of the plant cells could not be ascertained because of electron beam damage to the organic matter. The Pb-P grains tend to be

present in small groups in the ion-thinned sections (Fig. 3*a,c*) and are themselves aggregates of ~1 µm across, composed of numerous circular granules with diameters of ~50 nm (Fig. 3*b,d*). In order to determine the composition of the Pb-P grains, the EDX spectrum of a grain in the sample of ashed root was compared with the synthetic pyromorphite standard (Fig. 2). Identical conditions for background subtraction and peak stripping were used for both the sample and standard. Both spectra show the presence of Pb, P, Cl and O; minor amounts of Fe are also present in the ashed root grain. Using the pyromorphite standard, the P/Cl atomic ratio of the phase in the ashed root was estimated to be 3.7. This is equivalent to 80 mol.% of pyromorphite if the sample is considered to be a member of a solid solution between pyromorphite and Pb-hydroxyapatite (Pb₅(PO₄)₃OH). This figure must be regarded as approximate because of the incomplete separation of the Pb M and Cl K peaks at ~2.3 keV in the spectrum and the variable thickness of the analysed grains.

The polycrystalline nature of these grains is reflected in the electron diffraction patterns obtained from ashed samples (Fig. 4). These consist of incomplete rings, indicating the presence of many different crystalline orientations. The radii (R) of individual rings were measured from photographic negatives and converted to d -spacings using the equation $dR = \lambda L$, where λL is a camera constant (determined by the gold standard as 3.954 nm mm). Although some of the rings were incomplete, faint or broad (Fig. 4), d -spacings were obtained and compared with those from the International Center for Diffraction Data (ICDD) Powder Diffraction File (Table 1). The best fits to these d -spacings were obtained with two very similar lead phosphates, pyromorphite (Pb₅(PO₄)₃Cl, also known as chloropyromorphite, ICDD file no. 19-701) and Pb-hydroxyapatite (Pb₅(PO₄)₃OH, also known as hydroxypyromorphite, ICDD file no. 24-586). The two strongest rings in the electron diffraction pattern occur at d -spacings of 0.299 and 0.289 nm. Close examination of the photographic negative under an optical magnifier revealed that the first of these rings is in fact a double ring although separate measurements were not possible. These d -spacings agree well with the ICDD d -spacings of the three strongest reflections of pyromorphite at 0.2985, 0.2959 and 0.2885 nm corresponding to 211, 112 and 300 (with the first two of these reflections being unresolved, see

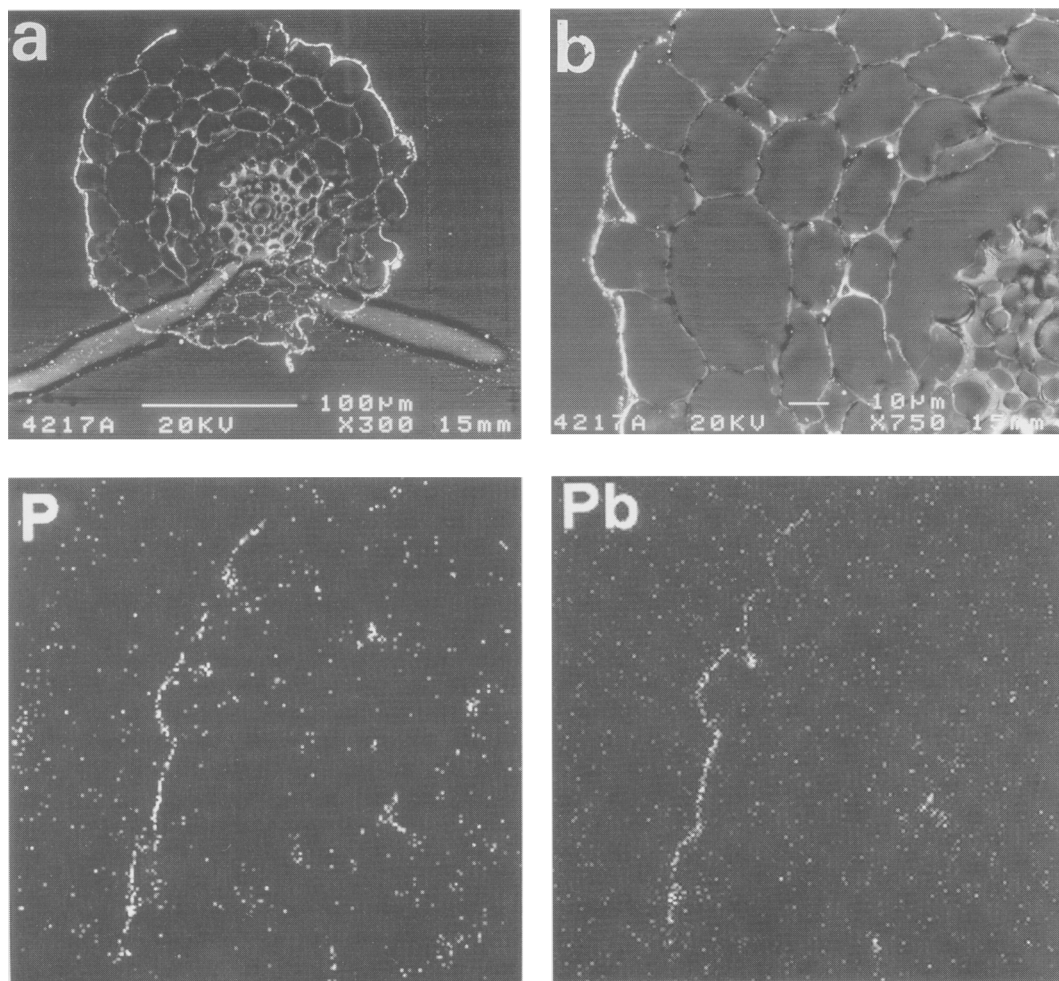


FIG. 1. Back scattered electron images (upper) of root sections indicating the presence of grains containing an element with high atomic number (bright areas) in the outer cell wall of the epidermis. (b) is an enlargement of (a). The P and Pb EDX maps (lower) of (b) show that these grains are Pb-rich and also contain P, indicating a Pb-P deposit. Grains containing P but not Pb could be Fe or Al phosphate.

Fig. 4) and also with the two strongest reflections of Pb-hydroxyapatite at 0.2974 nm (211 and 112, unresolved) and 0.2850 nm (300). It is not possible to distinguish between the two phases from these rings. However, the sharpest line of the pattern, and therefore the one that was most accurately measured, is that with a d -spacing of 0.328 nm (identified as 210). This d -value is much closer to the d -spacing of 210 for pyromorphite (0.327 nm) than for 210 of Pb-hydroxyapatite (0.324 nm). Thus, electron

diffraction supports the EDX evidence that the Pb-P grains are closer to pyromorphite in composition than to Pb-hydroxyapatite.

XAS

The X-ray absorption near edge structure (XANES) region of the XAS spectrum for the model compounds (Fig. 5) vary significantly. Comparison of these spectra with that of the root sample reveals features in the latter which are

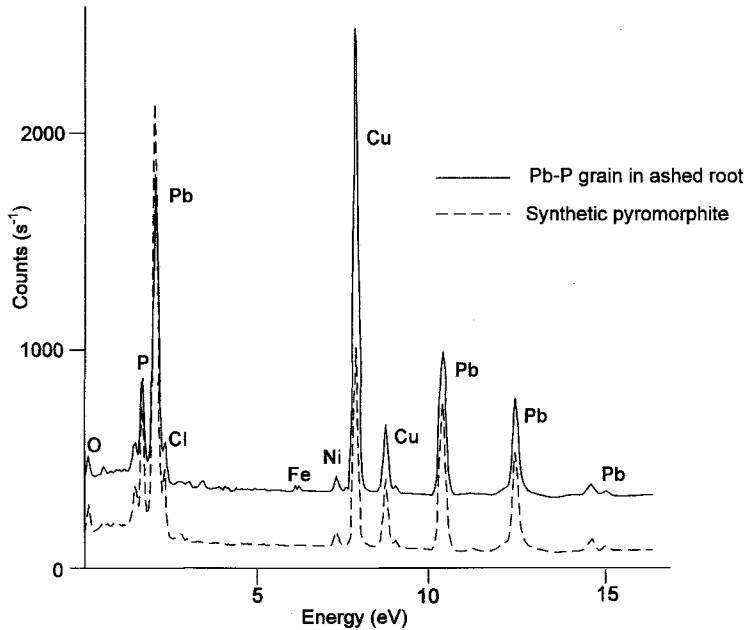


FIG. 2. ATEM EDX spectrum of a Pb-P grain from ashed root containing trace amounts of Fe and synthetic pyromorphite recorded under the same conditions. The copper peaks are from the support grid and the nickel peaks are from the coating on the pole pieces.

very similar to those of the Pb-hydroxyapatite and the pyromorphite spectra. However, the extended X-ray absorption fine structure (EXAFS) spectra revealed a closer similarity of the root spectrum to that of pyromorphite. The crystal structures of Pb-hydroxyapatite and pyromorphite (Table 2) are similar, but have some important differences. Only in pyromorphite is there the short (0.235 nm) Pb-O interaction and the Pb-Cl interaction at 0.311 nm. Analysis of the EXAFS spectrum of the plant roots showed that these shells needed to be included in order to get the best fit. Fitting the plant root spectrum using a model based on the first four shells of Pb-hydroxyapatite gave a fit with an R-factor of 42.7. Addition of a Pb-Cl interaction at 0.305 nm reduced the R-factor to 40.2, and the inclusion of a short Pb-O distance of 0.230 nm improved it further to 38.9, a significantly better fit indicating that pyromorphite is a better model for the plant root spectrum than Pb-hydroxyapatite. The EXAFS and corresponding Fourier transforms of pyromorphite and the root sample are compared in Fig. 6. These show close similarities, although the peaks

in the Fourier transform of the root sample are shifted to lower interatomic distances (r_{exafs}). The EXAFS parameters for pyromorphite and Pb-hydroxyapatite are compared with those derived from the root sample (using the same shells as pyromorphite) in Table 3. Fewer shells were observed for the roots because the data range was smaller, and the data too noisy at high k values (Fig. 6) to justify inclusion of shells beyond 0.35 nm. It is clear that the pattern of shells of backscatterers in the plant root are similar to those for pyromorphite, although the values of the absorber scatterer distances are consistently smaller for the Pb-P deposits in the roots, possibly due to surface effects arising from the very small size of the individual grains (Fig. 3). It is possible that the root sample contains a mixture of phases, including Pb-hydroxyapatite and pyromorphite, but the presence of the shells of O scatterers at 0.230 nm and the Cl scatterers at 0.305 nm, which both have Debye-Waller factors of similar magnitude to those in pyromorphite, and are absent for Pb-hydroxyapatite, implies that this phase is dominantly of a pyromorphite composition.

Pb-P GRAINS IN GRASS ROOTS

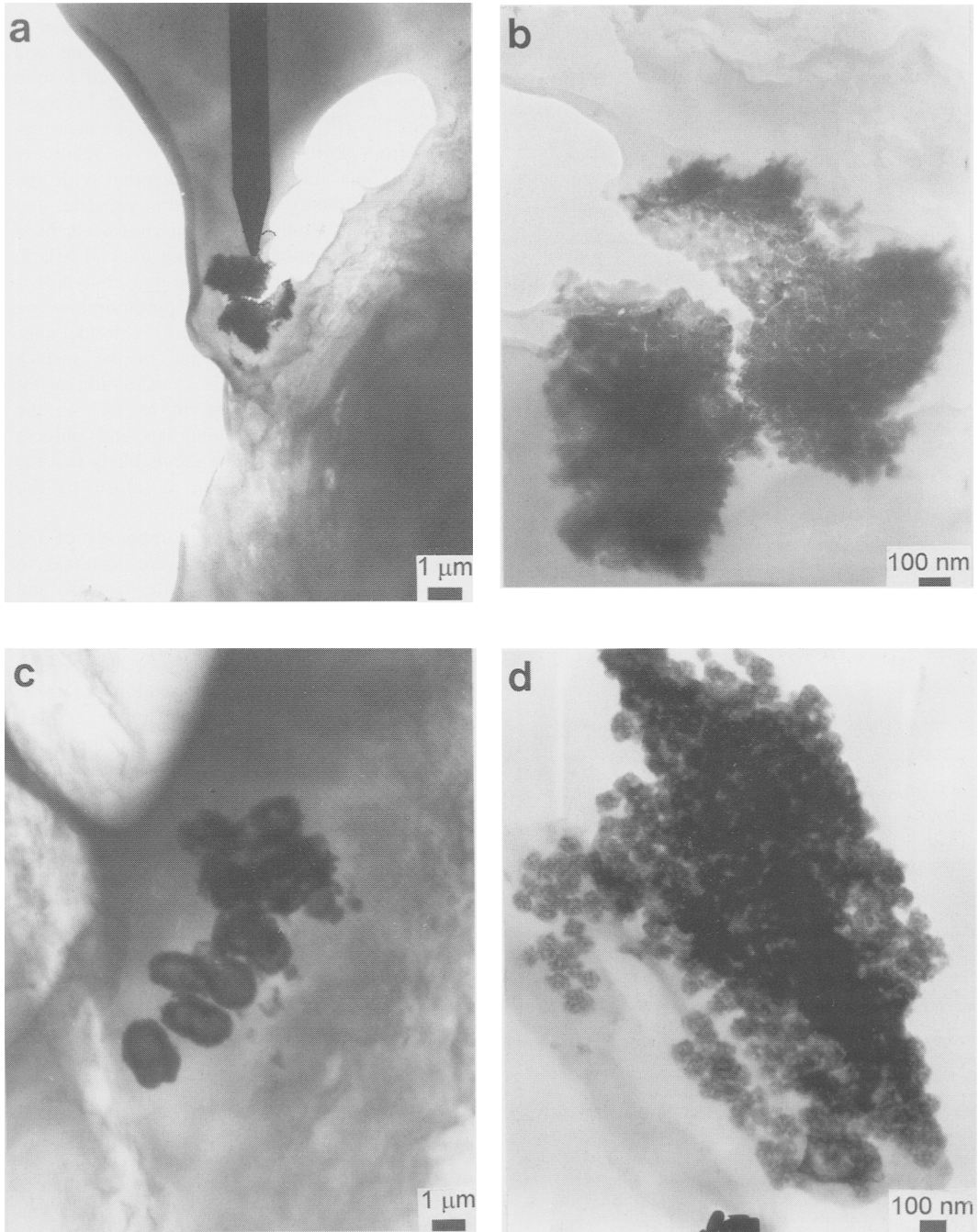


FIG. 3. Electron micrographs of Pb-P grains. (a), (b) and (c) are of ion thinned sections whilst (d) is from an ashed root. (b) is an enlargement of (c). The Pb-P grains tend to occur in clusters (a, c), whilst each grain is an aggregate composed of many smaller granules, (b, d).

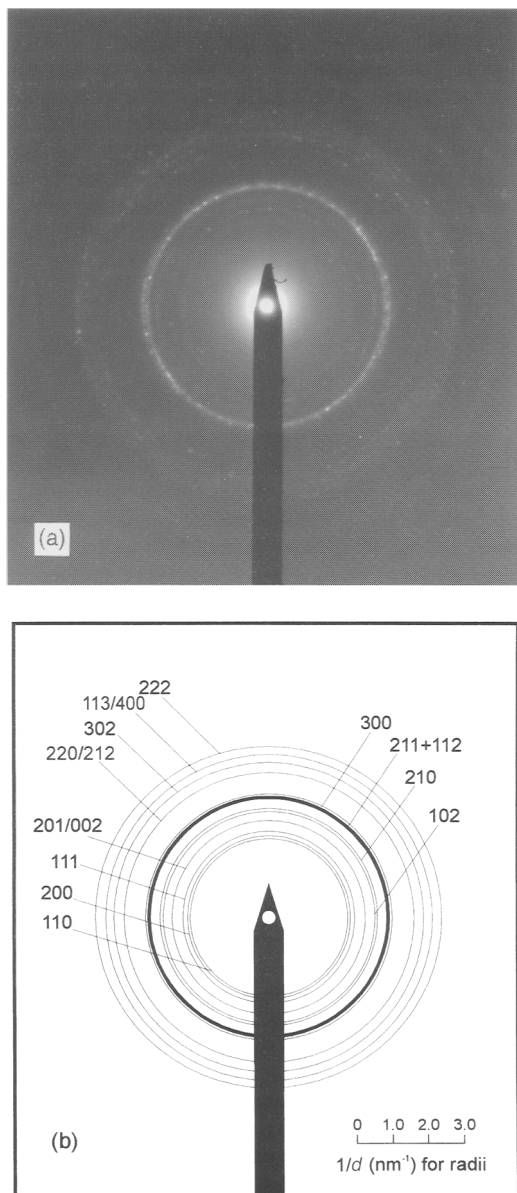


FIG. 4. *a* Selected-area electron-diffraction pattern and *b*) schematic from the Pb-P aggregate in Fig. 3*d*. The two most intense rings, corresponding to the (211) and (112) planes of both pyromorphite and Pb-hydroxyapatite, are not fully resolved by ATEM (see Table 1).

Discussion

The ATEM results combined with the EXAFS data provide strong evidence that these Pb-P

grains in the roots of *A. capillaris* have a pyromorphite ($\text{Pb}_5(\text{PO}_4)_3\text{Cl}$)-type structure and composition. The grains may be part of a solid solution between pyromorphite and Pb hydroxyapatite ($\text{Pb}_5(\text{PO}_4)_3\text{OH}$) but, if there is a contribution from Pb-hydroxyapatite, it is relatively minor. This finding is in keeping with the known chemistry of Pb-hydroxyapatite and pyromorphite. Pb-hydroxyapatite has never been reported as a naturally occurring mineral (Clark, 1993) and Nriagu (1974) found that Pb-hydroxyapatite rapidly converts to pyromorphite on exposure to solutions containing chloride ions. Chloride ions are ubiquitous in the surface environment and chlorine is a macro-nutrient for higher plants, mostly present as Cl^- in the aqueous phase, e.g. xylem sap and phloem (Marschner, 1995). Thus, it seems likely that the mineralogical composition is close to the pyromorphite end-member.

The size and aggregate morphology of the grains under ATEM (Fig. 3) are identical to those described previously (Cotter-Howells and Caporn, 1996), suggesting that pyromorphite grains are not a cause of, nor affected by, chemical fixation, freeze-drying or even ashing at 400°C. The aggregate morphology of these deposits contrasts with the smooth Zn-rich phytate globules of approximately the same size (1 µm diameter) observed in Zn-exposed roots by van Stevenick *et al.* (1987*a*; 1987*b*; 1990). Vázquez *et al.* (1994) found Zn-P grains of a similar size to the individual Pb-P grains in this study (~50 nm diameter) in the roots of *T. caeruleascens.*, but these did not form aggregates. Malone *et al.* (1974) found that the size of Pb-containing crystals increased with the length of Pb exposure but were usually 1–2 µm wide by 3–5 µm long.

The presence of the majority of pyromorphite grains in the outer wall of the epidermis (Fig. 1) agrees with earlier findings (Cotter-Howells and Caporn, 1996) that Pb-P grains could be removed from the root by ultrasound. Similarly, Vázquez *et al.* (1994) observed that Zn-P deposits were predominantly present in the epidermis and sub-epidermis of roots. However, the Zn-rich phytate globules found by van Stevenick (1987*a*; 1987*b*; 1990) were mostly located within the inner root (cortex). The identification of a crystalline phosphate phase, pyromorphite, in *A. capillaris* is in contrast to the phytate composition found by van Stevenick (1987*a*; 1987*b*; 1990) for Zn-P globules in *D. cespitosa* and *L. minor*. The

Pb-P GRAINS IN GRASS ROOTS

TABLE 1. Comparison of ICDD and observed (electron diffraction) *d*-spacings for pyromorphite and Pb-hydroxyapatite (Fig. 4)

Observed <i>d</i> -spacing nm ^a	Pyromorphite (ICDD file no. 19-701)			Pb-hydroxyapatite (ICDD file no. 24-586)		
	<i>hkl</i> ^b	ICDD <i>d</i> -spacing nm	Relative X-ray intensity	<i>hkl</i> ^b	ICDD <i>d</i> -spacing nm	Relative X-ray intensity
0.453	110	0.499	8	110	0.493	6
0.439	200	0.433	20	200	0.428	40
0.416	111	0.413	45	111	0.411	40
0.368	{ 201 002	0.373 0.367	2 8	— 002/201	— 0.371	— 6
0.337	102	0.338	25	102	0.341	40
0.328	210	0.327	35	210	0.324	40
0.299	{ 211 112	0.2985 0.2959	100 100	— 112/211	— 0.2974	— 100
0.289	300	0.2885	60	300	0.2850	45
n.o.	—	—	—	202	0.2803	4
n.o.	—	—	—	301	0.2660	2
n.o.	220	0.2497	2	220	0.2469	4
0.246	212	0.2440	2	212	0.2442	2
n.o.	—	—	—	310	0.2373	4
n.o.	—	—	—	n.i.	0.2343	2
0.230	302	0.2266	6	311/302	0.2263	6
0.219	{ 113 400	2.195 2.162	16 8	{ 113 400	0.2214 0.2139	10 8
0.206	222	2.063	35	222/401	0.2056	30

^a diffraction rings with *d*-spacings <0.2 nm were not measured as they were very faint.

^b braces indicate pairs of rings that would be too close to be differentiated in the electron diffraction pattern.

n.i. = not indexed

n.o. = not observed

TABLE 2. Comparison of the radial distribution around Pb (averaged over two sites in both cases) derived from the crystal structures of Pb-hydroxyapatite (Brückner *et al.*, 1995) and pyromorphite (Dai and Hughes, 1989)

Type of atom	Pb-hydroxyapatite		Pyromorphite	
	N _{cryst} ^a	<i>r</i> /nm ^b	N _{cryst} ^a	<i>r</i> /nm ^b
O	—	—	0.5	0.235
O	1.5	0.257	1.5	0.256
O	4	0.264	3.5	0.267
O	3	0.295	2	0.294
Cl	—	—	1	0.311
P	2.5	0.335	2	0.334
P	—	—	2.5	0.371
Pb	1	0.371	1	0.376
P	3	0.384	1	0.395

^a N_{cryst} is the number of atoms

^b *r* is the interatomic separation distance.

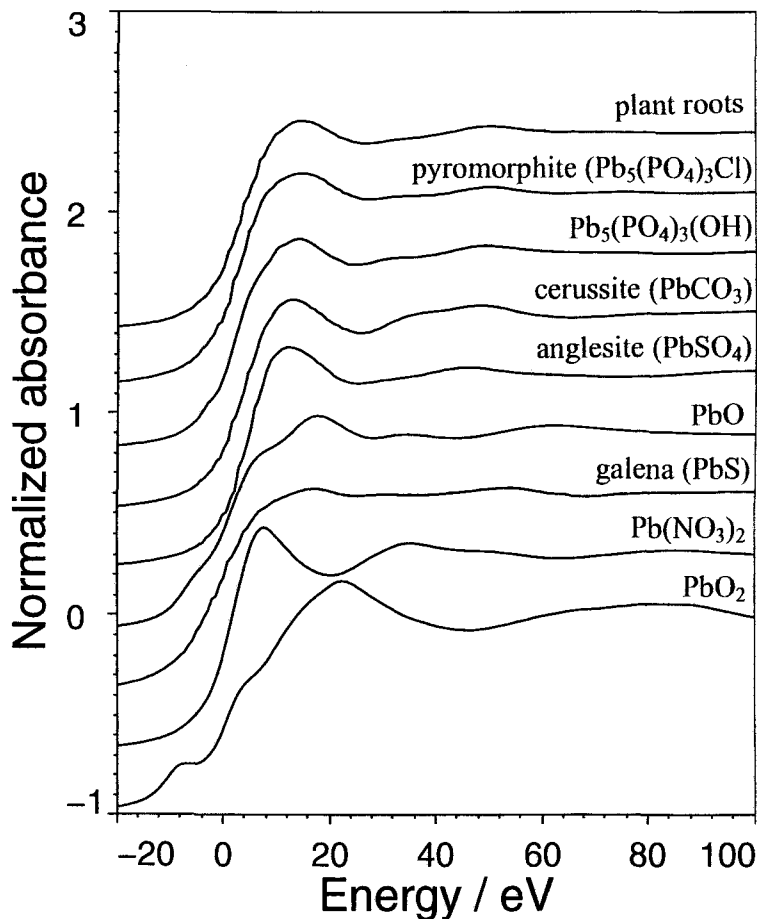


FIG. 5. XANES spectra from freeze-dried roots and a range of model (pure) lead compounds. Note the similarity of the pyromorphite and Pb-hydroxyapatite ($\text{Pb}_5(\text{PO}_4)_3(\text{OH})$) spectra with that of the plant roots.

identification of different compounds for Zn and Pb may reflect differences in chemistry between the two elements. However, a lack of published thermodynamic data for heavy metal phytate compounds prevents development of complete models for the different systems.

It is evident that there is variation in the morphology, chemical composition and transverse location of heavy metal deposits within plant roots. Whilst some of this variation may be accounted for by differences between studies, e.g. exposure of plants to different concentrations of heavy metals, examination of differing plant species and of different root portions, the lack of similarities suggests that different types of heavy metal P deposits occur in plant roots, even for the same

element. Therefore, detailed micro-mineralogical studies such as the present study are of vital importance in determining the nature and structural composition of these heavy metal deposits. This will eventually allow systematic comparisons between different plant species and elements.

The physiological role of pyromorphite precipitation in roots is unclear. *A. capillaris* cv. Parys Mountain is tolerant to Pb, Cu and Zn and it is possible that the deposits are part of a tolerance mechanism. Certainly the precipitation of pyromorphite would prevent Pb from interfering with plant metabolism, thereby detoxifying Pb within the plant. Van Stevenick *et al.* (1987b) found more Zn-rich phytate globules in a Zn-tolerant ecotype of *D. cespitosa* than in a non-tolerant

TABLE 3. Comparison of the best fit EXAFS simulation parameters for the Pb L(III)-edges of Pb-hydroxyapatite, pyromorphite and plant root

Type of atom	Pb-hydroxyapatite		Pyromorphite		Plant root		
	N_{cryst}	$r_{\text{exafs}}/\text{nm}^a$	$10^2 2\sigma^2/\text{nm}^2$ ^b	Type of atom	N_{cryst}	$r_{\text{exafs}}/\text{nm}^a$	$10^2 2\sigma^2/\text{nm}^2$ ^b
O	1.5	0.252	0.029	O	0.5	0.232	0.000
O	4	0.263	0.052	O	1.5	0.251	0.008
O	3	0.295	0.041	O	3.5	0.271	0.029
				Cl	2	0.304	0.010
P	2.5	0.354	0.055	P	1	0.306	0.014
Pb	1	0.366	0.044	P	2	0.346	0.067
P	3	0.391	0.038	Pb	2.5	0.379	0.026
				P	1	0.378	0.009
					1	0.406	0.002
						— ^c	—
						—	—
						—	—

^a r_{exafs} is the absorber-scatterer distance, ± 0.002 nm inner coordination sphere, ± 0.005 nm outer shells.

^b $2\sigma^2$ is the Debye-Waller factor, $\pm 25\%$.

^c EXAFS spectrum is too noisy at high k values to determine outer shell radii (see Fig. 6).

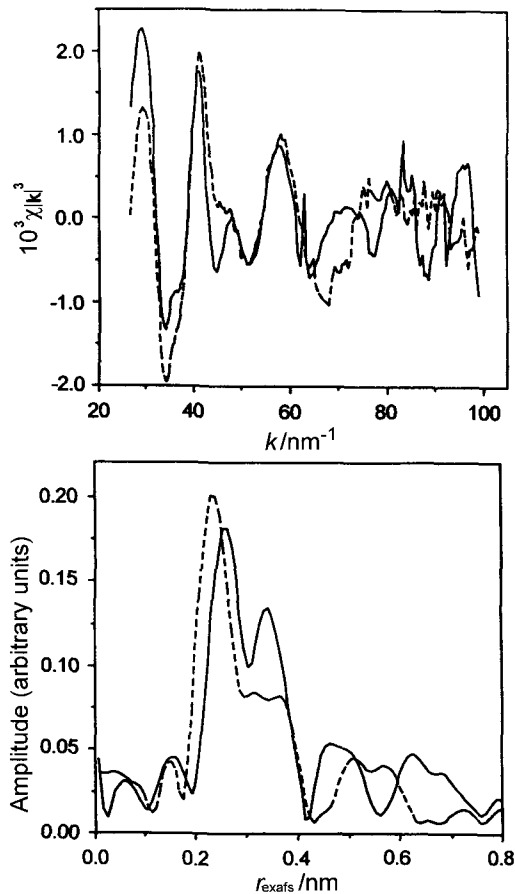


FIG. 6. Comparison of EXAFS spectra (above) from freeze-dried roots (dashed) and pyromorphite (solid) together with associated phase-shift corrected Fourier transforms (below).

ecotype, leading the authors to suggest that the association of Zn with phytate could act as a tolerance mechanism. However, the supply of P to the plant must also be considered. Phosphorus precipitated with a heavy metal is no longer available for metabolic function which could result in P deficiency in the plant.

The toxicity/tolerance arguments presented for plants also extend to phosphatic deposits observed in other organisms. These deposits have been implicated in metal detoxification mechanisms for invertebrates such as snails and protozoa (Simkiss and Taylor, 1989). Low molecular weight S-binding proteins (phytochelatins in plants and metallothioneins in animals) have recently been

studied intensively. They are thought to play an important role in the detoxification of heavy metals through complexation (Rausser, 1990; Posthuma and Straalen, 1993). However, it is currently becoming accepted that these proteins do not represent an exclusive detoxification mechanism (e.g. Krämer *et al.*, 1996) and that other detoxification mechanisms also exist, in some instances in conjunction with S-binding proteins (Rausser, 1990; van Stevenick, 1987b).

Conclusions

Pb-P deposits in the roots of a heavy metal ecotype of a grass species, *A. capillaris* have a structure and composition indicative of pyromorphite, $Pb_5(PO_4)_3Cl$, although there may be substitution of some of the Cl by OH. The majority of pyromorphite grains were present in the outer wall of the epidermis with individual polycrystalline grains (~50 nm diameter) clustering to give aggregates of 1 μm diameter. Comparison with heavy metal deposits observed in other plant studies is difficult because the precise nature of many of these deposits is not known. However, the phosphate composition of these grains does appear to contrast with the phytate composition of Zn-P deposits. The physiological role of these deposits remains unclear; the precipitation of heavy metal P compounds in plants could be a detoxification mechanism or simply a passive, antagonistic reaction between heavy metals and P.

Acknowledgements

This work was supported by NERC fellowship GT5/AAPS/92/1, awarded to J.C.H. We are grateful to CLRC Daresbury Laboratory for provision of beam-time. Lynne Robertson assisted in preparation of the standards and the photographs were printed by Norman Little. We thank the referees for providing helpful comments and suggestions.

References

- Allen, S.E. (1989) *Chemical Analysis of Ecological Materials*. Blackwell Scientific, Oxford.
- Binsted, N., Campbell, J.W., Gurman, S.J. and Stephenson, P.C. (1991) *SERC Daresbury Laboratory EXCURV92 Program*. Daresbury Laboratory, Warrington, UK.
- Binsted, N., Strange, R.W. and Hasnain, S.S. (1992)

- Constrained and restrained refinement in EXAFS data analysis with curved wave theory. *Biochem.*, **31**, 12117–25.
- Brückner, S., Lusvardi, G., Menabue, L. and Saladini, M. (1995) Crystal structure of lead hydroxyapatite from powder X-ray diffraction data. *Inorg. Chim. Acta*, **236**, 209–12.
- Charnock, J.M. (1995) Biological applications of EXAFS spectroscopy. *Radiat. Phys. Chem.*, **45**, 385–91.
- Clark, A.M. (1993) *Hey's Mineral Index: Mineral Species, Varieties and Synonyms*. (3rd edition). Chapman & Hall, London.
- Cotter-Howells, J.D. (1996) Lead phosphate formation in soils. *Environ. Poll.*, **93**, 9–16.
- Cotter-Howells, J.D. and Caporn, S.J. (1996) Remediation of contaminated land by formation of heavy metal phosphates. *Appl. Geochem.*, **11**, 335–42.
- Cotter-Howells, J.D., Champness, P.E., Charnock, J.M. and Patrick, R.A.D. (1994) Identification of pyromorphite in mine-waste contaminated soils by ATEM and EXAFS. *Eur. J. Soil Sci.*, **45**, 393–402.
- Dai, Y. and Hughes, J.M. (1989) Crystal structure refinements of vanadinite and pyromorphite. *Canad. Mineral.*, **27**, 189–92.
- Davis, A., Drexler, J.W., Ruby, M.V. and Nicholson, A. (1993) Micromineralogy of mine wastes in relation to lead bioavailability, Butte. *Environ. Sci. Technol.*, **27**, 1415–25.
- Krämer, U., Cotter-Howells, J.D., Charnock, J.M., Baker, A.J.M. and Smith, J.A.C. (1996) Free histidine as a metal chelator in plants that accumulate nickel. *Nature*, **379**, 635–8.
- Ma, Q.Y., Logan, T.J. and Traina, S.J. (1995) Lead immobilisation from aqueous solutions and contaminated soils using phosphate rocks. *Environ. Sci. Technol.*, **29**, 1118–26.
- Malone, C. Koepe, D.E. and Miller, R.J. (1974) Localisation of lead accumulated by corn plants. *Plant Physiol.*, **53**, 388–94.
- Marschner, H. (1995) *Mineral Nutrition of Higher Plants*. (2nd edition). Academic Press, London.
- Nriagu, J.O. (1974) Lead orthophosphates-IV. Formation and stability of chloropyromorphite at 25°C. *Geochim. Cosmochim. Acta*, **37**, 367–77.
- Nriagu, J.O. (1984) Formation and stability of base metal phosphates in soils and sediments. In *Phosphate Minerals* (J.O. Nriagu and P.B. Moore, eds). Springer-Verlag, London, pp. 318–29.
- Nriagu, J.O. and Moore, P.B., Eds (1984) *Phosphate Minerals*. Springer-Verlag, London.
- Posthuma, L. and Straalen, N.M.V. (1993) Heavy-metal adaptation in terrestrial invertebrates: a review of occurrence, genetics, physiology and ecological consequences. *Comp. Biochem. Physiol.*, **106C**, 11–38.
- Rausser, W.E. (1990) Phytochelatins. *Ann. Rev. Biochem.*, **59**, 61–86.
- Ruby, M.V., Davis, A. and Nicholson, A. (1994) *In situ* formation of lead phosphates in soils as a method to immobilize lead. *Environ. Sci. Technol.*, **28**, 646–54.
- Simkiss, K. and Taylor, M.G. (1989) Convergence of cellular systems of metal detoxification. *Marine Environ. Res.*, **28**, 211–14.
- Turnau, K., Kottke, I. and Oberwinkler, F. (1993) Element localisation in mycorrhizal roots of *Pteridium aquilinum* (L.) Kuhn collected from experimental plots treated with cadmium dust. *New Phytol.*, **123**, 313–24.
- van Steveninck, R.F.M., van Steveninck, M.E., Fernando, D.R., Godbold, D.L., Horst, W.J. and Marschner, H. (1987a) Identification of zinc containing globules in roots of a zinc tolerant ecotype of *Deschampsia cespitosa*. *J. Plant Nutr.*, **10**, 1239–46.
- van Steveninck, R.F.M., van Steveninck, M.E., Fernando, D.R., Horst, W.J. and Marschner, H. (1987b) Deposition of zinc phytate in globular bodies in roots of *Deschampsia cespitosa* ecotypes; a detoxification mechanism? *J. Plant Physiol.*, **131**, 247–57.
- van Steveninck, R.F.M., van Steveninck, M.E., Wells, A.J. and Fernando, D.R. (1990) Zinc tolerance and the binding of zinc as zinc phytate in *Lemna minor*. X-ray microanalytical evidence. *J. Plant Physiol.*, **137**, 140–6.
- Vázquez, M.D., Poshenrieder, Ch., Barceló, J., Baker, A.J.M., Hatton, P. and Cope, G.H. (1994) Compartmentation of zinc in roots and leaves of the zinc hyperaccumulator *Thlaspi caerulescens* J. and C. Presl. *Bot. Acta*, **107**, 243–50.

[Manuscript received 8 September 1997;
revised 15 March 1999]